VDMA
Fluid Power Association

23rd ISC

International Sealing Conference

Stuttgart, Germany
Sept.30 - Oct.1, 2026

Sealing the future –
Facing the challenges of tomorrow

UNI STUTTGART

Fachverband Fluidtechnik im VDMA e. V. Lyoner Str. 18
50628 Frankfurt am Main
Germany

Phone +49 69 6603-1513
E-Mail maximilian.baxmann@vdma.eu

Internet www.vdma.eu/fluid

From Test Samples to Rotary Shaft Seals: A Numerical Approach for Wear Prediction

Jacqueline Gerhard, Frank Bauer

Rotary shaft seals are critical components in mechanical engineering, and failure due to wear can lead to costly system breakdowns. In order to numerically predict wear of sealing rings, a method was developed that uses finite element analysis and a subroutine to determine wear between two contact bodies, as well as to iteratively implement volume reduction due to wear. The main objective of this study was to identify a suitable wear coefficient by testing the wear on material samples using a measuring device, and to demonstrate the influence of test data and the resulting wear coefficient on wear predictions.

1 Introduction

To numerically predict the wear of rotary shaft seals, a method using subroutines in the finite element (FE) analysis software Marc/Mentat was developed. This numerical approach uses the FE Method to compute the contact pressure between two contact bodies. Based on this pressure, the subroutine uses a wear model to iteratively implement material removal due to wear. The wear model mathematically describes the wear behavior and contains at least one material-dependent wear coefficient that must be determined experimentally.

In this study, a wear model containing a single wear coefficient was employed. This coefficient was determined through experiments in which a material sample is pressed against a rotating shaft. The main difficulty with wear prediction in general, lies in defining these wear coefficients. Therefore, in the numerical method, the geometry of the test sample used in the experiments and the setup of the measuring device were considered first. The wear measured after the experiments was then compared with the numerically determined wear to validate the experimentally determined wear coefficient. This process identified and resolved difficulties and potential sources of error in determining the wear coefficients.

The following section introduces well-known wear models. This is followed by a description of the software used and the subroutine implemented to apply wear in the FE analysis. The process of determining the wear coefficients is then explained.

1.1 Wear models

A wear model describes material loss due to wear using a mathematical formula, making it essential for numerical wear calculations.

According to Fleischer [1], the wear height

$$d_{\mathrm{wear}} = \frac{1}{e^*}\, p_{\mathrm{N}}\, \mu\, s \tag{1}$$

depends on the contact pressure p_{N} acting normal to the surface, the sliding distance s, the coefficient of friction μ and the hypothetical friction energy density e^{*}. The hypothetical friction energy density includes the wear volume V_{wear} and the friction work W_{fric} and relates the work performed on the tribological system to the wear volume [2]. Since this hypothetical friction energy density e^{*} in Fleischer's energetic model is difficult to determine, Archard's wear model

$$d_{\mathrm{wear}} = \frac{K}{H}\ p_{\mathrm{N}}\ s, \tag{2}$$

with a linear relationship between the wear height and the contact normal pressure, is often used. This wear model assumes that the wear depth is determined solely by the contact pressure p_{N}, distance travelled s and material hardness H. The wear coefficient K is defined by fitting the wear equation to experimental data and therefore depends on the tribological system.

A generalization of Archard's wear law is represented by Bayer's exponential form

$$d_{\mathrm{wear}} = k_{b1}\ {p_{\mathrm{N}}}^{k_{b2}}\ {v_{\mathrm{rel}}}^{k_{b3}}\ s \tag{3}$$

that uses two exponents k_{b2} and k_{b3} to describe the nonlinear relationship between wear depth and normal pressure, as well as wear depth and relative velocity v_{rel}. This exponential form was further optimized, resulting in the Bayer exponential form with thermal activation, which additionally considers the temperature effect on the wear rate.

Haiser [3] analyzed the linear relationship between contact pressure and wear volume for different polytetrafluoroethylene materials (PTFE) and counterfaces. He observed that the linear relationship, as applied in Archard's wear law, is valid only up to a certain contact pressure. At higher pressures, the wear increases disproportionately. In order to be able to model the wear at a higher normal pressure, Weber [4] introduced the exponential relationship

$$d_{\mathrm{wear}} = k_{w1}\ exp(k_{w2}\ p_{\mathrm{N}})\ s \tag{4}$$

by replacing the normal pressure in Archard's wear law with a natural exponential function using an additional coefficient.

Many other models of varying complexity are presented in literature. Depending on the wear model, a different number of coefficients must be determined by fitting the wear model to experimental data. The accuracy of the numerical prediction of wear depends on the accuracy of the wear coefficients, regardless of how detailed the wear model is or how many influencing factors it takes into account. Thus, the greatest challenge in determining wear numerically is defining these wear coefficients. Rather than developing a highly complex wear model capable of accounting for all possible influences, this study focused on determining the wear coefficient as accurately as possible. Therefore, many experiments with test samples have been performed using the measuring device described in [5] to define the material-dependent wear coefficients using the procedure explained in the following.

Reformulating equation (2) yields the Archard model's wear coefficient

$$K = \frac{d_{\text{wear}}\,H}{p_{\text{N}}\,\,\,s}\ . \tag{5}$$

When the hardness H of the material being tested is given in N/mm², the wear coefficient K is a dimensionless quantity.

This study focuses only on a single material, which is a fluorocarbon rubber (FKM) with a hardness of 75 Shore A; Shore being the commonly used unit for the hardness of an elastomer. Due to focusing on only one material, a wear coefficient

$$\tilde{K} = \frac{d_{\text{wear}}}{p_{\text{N}}\,\,\,s}\ , \tag{6}$$

which is independent of the material's hardness, is used. The rotational speed and test duration are defined beforehand, which allows the distance traveled s to be calculated. After the test, the wear depth d_{wear} must be measured.

1.2 Software and Subroutine

The FE model was built using the MSC Marc/Mentat software, which consists of the solver Marc and the pre- and post-processor Mentat. Mentat is a graphical user interface (GUI) through which the solver Marc can be launched. Figure 1 shows an illustration of the communication between the GUI Mentat and the solver Marc.

In the pre-processor, the geometry was imported and meshed. The contact bodies, boundary conditions and load cases were then defined. Once the FE model has been set up in the GUI Mentat, the solver Marc is started to solve the underlying system of equations numerically. After a successful calculation, the results can be analyzed in the post-processor of the GUI Mentat.

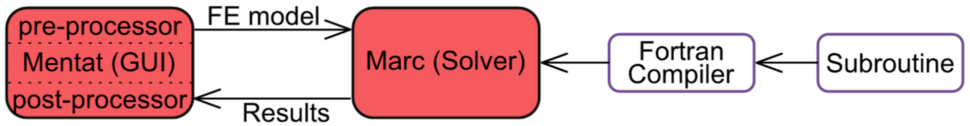

Figure 1: Software Framework and Interface Overview

A Fortran user subroutine was used to calculate and implement wear on designated contact bodies in the FE analysis, which requires a Fortran compiler. This subroutine only communicates with the solver Marc. A wear model implemented in the subroutine determines how the solver calculates the wear depth d_{wear} of each node in the FE model.

When building the FE model, so-called load cases were used to define what happens during the analysis. These load cases, for example, are *mounting*, *rotating shaft* and *demounting*. After setting up the FE model, the solver Marc divides each load case into a predefined number of increments. In each increment, the wear subroutine is executed for all nodes of the FE model that are in contact. The implemented subroutine consists of the following steps:

- **Increment-based Filtering:** To optimize performance, wear is only evaluated during relevant analysis stages. For instance, the subroutine is bypassed during the load case *mounting* and only activated for the load case *rotating shaft*.
- **Spatial Restriction (Contact Pair Selection):** Only nodes of a specified contact pair are considered. Although the solver identifies all nodes in contact, the subroutine filters these, focusing only on the relevant contact pair (e.g., the shaft-seal contact).
- **Wear model:** The core of the Fortran subroutine allows for the implementation of custom wear equations, providing the flexibility to adapt the wear height equations as required.

Figure 2 shows a two-dimensional schematic example of an FE model comprising two rigid contact bodies, CB_{load} and CB_{shaft}, and the meshed contact body CB_{meshed}, to which wear is applied, resulting in a reduction in volume. The meshed contact body (CB_{meshed}) consists of six rectangular elements and is positioned between two counter bodies (CB_{load} and CB_{shaft}), which are modelled as lines. A force is applied to CB_{load}, pressing the meshed contact body against CB_{shaft}, which moves at a relative velocity and represents the shaft. In Figure 2 (a), the meshed contact body CB_{meshed} has not yet come into contact with either of the two other bodies. Figure 2 (b) shows the situation after CB_{load} was pressed downwards, bringing all three bodies into contact. Consequently, the wear height d_{wear} is now calculated in the Fortran subroutine for the six nodes in contact, using the predefined wear model.

As there is no relative velocity between CB_{meshed} and CB_{load}, the resulting wear height for these three nodes is zero. For the three nodes in contact with CB_{shaft}, however, the wear height is greater than zero, and the nodes are moved upwards, Figure 2 (c). As the contact pressure between CB_{meshed} and CB_{shaft} is the same for all three nodes, the wear height is also the same for all three nodes. Since the meshed contact body is pressed down by CB_{load}, the contact between CB_{meshed} and CB_{shaft} is then re-established, Figure 2 (d).

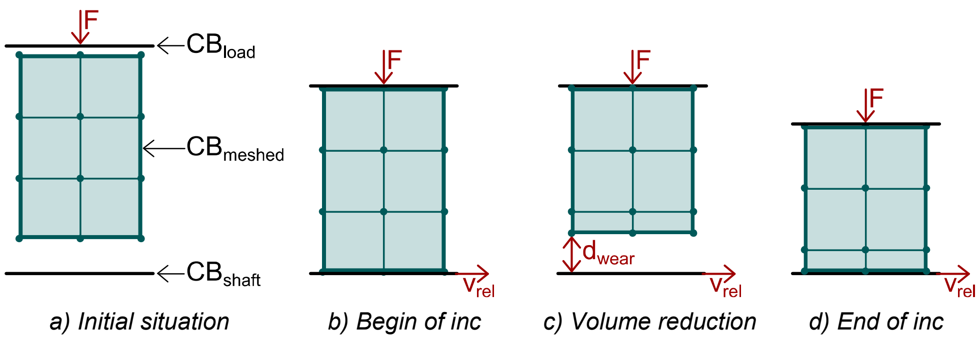

Figure 2: Application of wear and, as a result, volume reduction on an example model

1.3 Experiments

A Brugger lubricant tester in accordance with DIN 51347 was modified as described in [5] to enable the testing of materials used in sealing technology. Test runs were performed on samples of 2 mm-thick fluorocarbon rubber (FKM) sheet material using this measuring device, following the procedure explained in [5]. During these tests, a lever mechanism with an attached 200 g weight pressed the 2 mm-thick material sample onto a 25 mm-diameter shaft, applying a normal force of 25 N between the sample and the shaft. The shaft then rotates at 1,500 rpm for a predefined duration, corresponding to a relative velocity of 1.96 m/s between the shaft and the sample. For determining the wear coefficients of sealing materials, this test setup has many advantages over alternative methods, such as a pin-on-disc tribometer. One advantage is that the hydrodynamics and tribological conditions between the material sample and the shaft resemble those in a typical sealing application. As with the sealing edge of a rotary shaft seal, the contact area increases over time due to wear, resulting in a decrease in contact pressure.

The numerical model detailed in Section 2.1 was first validated using experimental tests conducted without lubrication due to accelerated wear resulting from the high coefficient of friction in dry contact. Figure 3 shows the average wear depths of FKM samples tested without lubrication. Nine test durations were considered, with three tests performed for each duration and new samples used for each test. The error bars in Figure 3 indicate the standard deviation of the three test runs per distance travelled.

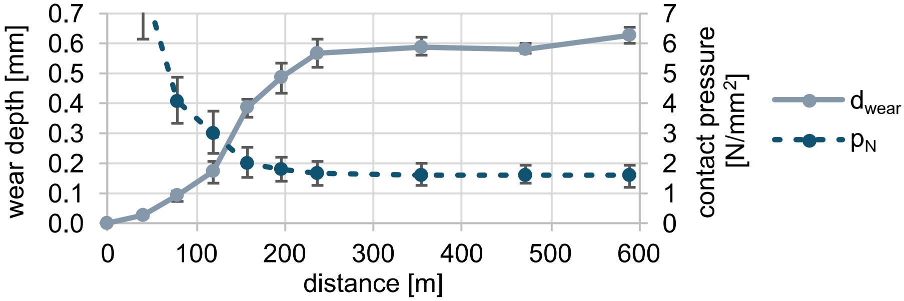

Figure 3: Test results with FKM samples: wear depth and contact pressure

The wear depths d_{wear} were measured using the IMA-Sealscanner [6]. To determine the contact pressure, the wear area A_{wear} was measured after testing using a digital microscope, detailed in [5]. The contact pressure was then calculated based on the measured wear area. In tests over short distances, the measured wear area on the samples remained small, resulting in a high calculated contact pressure. Due to wear, the contact area increases during the test. The 5 mm width of the material samples limits the width of the contact area. Consequently, the contact area increases only slightly from a distance of approximately 300 m onwards, meaning that the contact pressure also decreases only slightly.

It is well known that the wear rate is not constant over time and that three phases can be distinguished in an idealized friction contact over its service life. The first phase, known as the running-in phase, is characterized by a relatively high wear rate that decreases rapidly. In the second phase, wear increases at a lower, constant rate. The third phase occurs at the end of the service life and is characterized by progressive wear. Therefore, it was expected that wear would increase rapidly at first before levelling off into a linear increase. However, as Figure 3 shows, wear increased slowly at first, which could be due to low starting temperatures.

A thermal imaging camera was used to record the temperatures at the contact area during the experiments, as discussed in [5]. At the start of a test run, both contact surfaces are at ambient room temperature. Due to the high dry sliding friction at v_{rel} = 1.96 m/s, rapid frictional heating occurred, leading to surface temperatures of up to 125 °C before a thermal quasi-steady state was reached [5].

Elastomers exhibit strong temperature-dependent mechanical and tribological behavior: at lower initial temperatures, the material is stiffer and less susceptible to thermal degradation, resulting in a lower initial wear rate. However, as the contact temperature rises, thermal softening and accelerated material loss due to wear result in an increasing wear rate, peaking after approximately 200 m before stabilizing at a lower wear rate.

1.4 Wear coefficients

Based on the wear depths and contact pressures shown in Figure 3, a wear coefficient was calculated according to equation (6) for each of the nine distances tested. The resulting wear coefficients for the FKM-steel friction pair under non-lubricated conditions are shown in Figure 4. With the normal pressure in N/mm², wear depth in mm, and the distance in mm, the wear coefficient calculated using equation (6) is given in units of mm²/N. This unit refers to the system of units used in this analysis and will not be mentioned again.

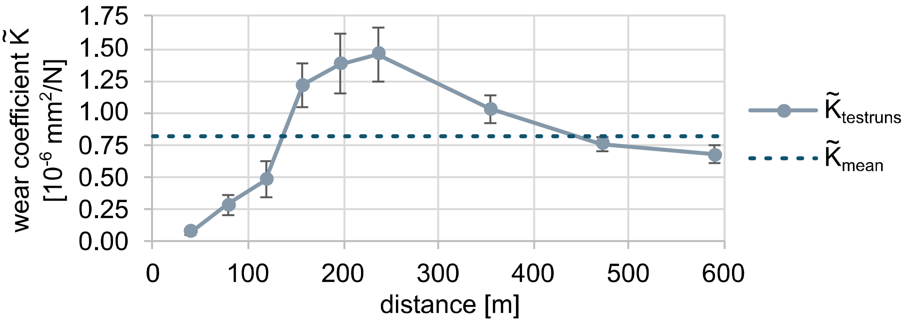

Figure 4: Wear coefficients calculated based on the test results

The distance tested in the experiments and the contact area measured after the tests significantly impact the calculated wear coefficient. To accurately account for this non-constant wear behavior, a time-dependent wear coefficient could be implemented. However, this approach would likely result in overfitting of the numerical model and was therefore not considered further. Instead, to analyze the effect on the results of the FE analysis, three different wear coefficients were considered:

- $\widetilde{K}_{\mathrm{t20}}$: Based on shortest test runs after s = 39 m (or 20 seconds of testing)
- $\widetilde{K}_{\mathrm{t120}}$: Greatest wear coefficient after s = 236 m (or 120 seconds of testing)
- $\widetilde{K}_{\mathrm{t300}}$: Based on longest test runs after s = 589 m (or 300 seconds of testing)
- $\widetilde{K}_{\mathrm{mean}}$: The wear coefficient shown in Figure 4 was integrated over s = [39 m, 589 m] and divided by 550 m to obtain the mean value

The lower wear coefficient at the start of the test could be due to low initial temperatures. Therefore, using the wear coefficient $\widetilde{K}_{\mathrm{t20}}$ would lead to erroneously low wear results. The longest test run is generally assumed to provide the most accurate basis for determining the wear coefficient since, by that point, the temperature in the contact area will have stabilised at around 125 °C and the wear coefficient is not expected to be overestimated due to the higher wear rate during the running-in phase.

Table 1 shows the calculated wear coefficients, as well as the values used in the calculation. The four wear coefficients $\widetilde{K}_{\mathrm{t20}}$, $\widetilde{K}_{\mathrm{t120}}$, $\widetilde{K}_{\mathrm{t300}}$, and $\widetilde{K}_{\mathrm{mean}}$ were used in the FE analysis of the test setup used for the experiments. Comparing the results of the FE analysis with the experimental data showed which wear coefficient is best suited for the application.

Table 1: Calculated wear coefficients for the FE analysis

	t = 20 s	t = 120 s	t = 300 s	t = [20 s, 300 s]
d_{wear} [mm]	0.024	0.57	0.62	
p_{N} [N/mm^2]	8.07	1.65	1.57	
s [m]	39.27	235.62	589.05	
$\widetilde{K}$ [10^{-6} mm^2/N]	0.076	1.457	0.677	0.820

2 Validation of the wear coefficient

In order to reproduce the wear resulting from the test runs in the numerical FE analysis, the measuring device used for the experiments was replicated as accurately as possible in an FE model. This model consists of the geometry of the FKM material sample and the rigid geometry of the shaft. A detailed description of the simulation setup is provided in the following subsection, followed by the presentation and discussion of the results.

2.1 Finite Element Analysis

Figure 5 (left) shows the FE model of the material sample, which is pressed against the rotating shaft. This setup is based on the configuration of the measuring device used for the experiments, detailed in [5]. The displacement of all nodes on the 'fixed surface' is fixed in all three directions. During the experiments, a normal force F_N was applied to the material sample in the negative y-direction. In the FE model, however, a force is applied to the shaft in the positive y-direction, since it is easier to apply a force to a rigid body than to a meshed body. Displacement of the shaft is fixed in the x- and z-directions, and the shaft rotates around the x-axis.

Figure 5 (right) shows the material sample with the initial mesh, consisting of 5,506 elements, which was generated in Mentat. Tetrahedral elements with four Gaussian integration points and the 'full and Hermann formulation' were used. As the nodes in contact with the shaft are shifted due to wear, some elements might become too distorted. As a result, the underlying mathematical equations may become inaccurate or fail entirely. To prevent this, the geometry is continuously remeshed, resulting in a finer mesh at the end of the simulation, Figure 8.

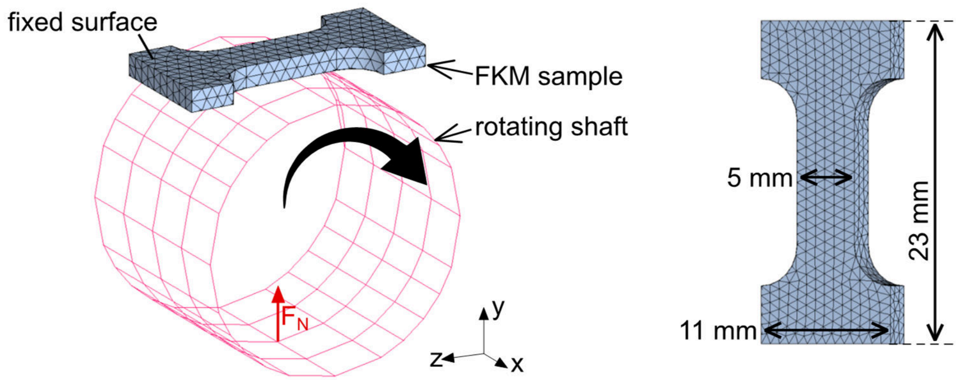

Figure 5: FE model (left) and FKM material sample (right)

Tensile tests at 100°C were carried out on S2 shoulder bars according to DIN 53504. Based on these tests, an Ogden material model was formulated. Therefore, in the numerical calculation, it is assumed that the temperature at each node of the material sample is 100 °C throughout the entire experiment. In reality, however, the tests began at room temperature and increased to 125 °C during the experiment [5].

The FE analysis considers three load cases:

- **Mounting**: A normal force of 25 N is applied to the shaft, pressing it upwards against the material sample. At the end of the load case, the geometry is re-meshed.
- **Rotating shaft**: The shaft rotates at 1,500 rpm, which corresponds to a relative velocity of 1.96 m/s. The mesh quality is checked after each increment. If the quality of an element is too poor, the area around the contact area is remeshed.
- **Demounting**: The shaft is moved downwards.

Figure 6 shows a side-on view of the meshed material sample at the start of the simulation and after 1 km of sliding distance. When severe distortion occurred, the mesh was remeshed around the contact area. Therefore, the elements further away from the contact area remain unchanged, whereas the elements in the center of the sample have changed.

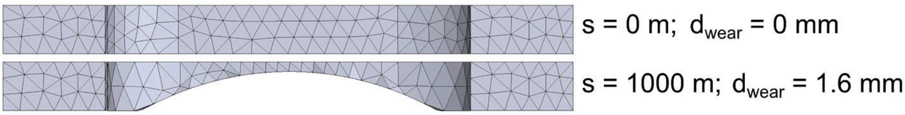

Figure 6: Material sample: Initial mesh without wear and remeshed sample with wear

2.2 Results

This section presents the results of the FE analysis: the wear depth and contact pressure, which were determined numerically, over the distance travelled. The FE model was computed for the four wear coefficients listed in Table 1. To compare the wear depth over distance traveled for the four different coefficients, the maximum wear depth value was stored every 10 meters. Figure 7 compares the maximum wear depth values resulting from the FE analysis with the experimental results. The lower x-axis shows distance travelled, and the upper x-axis shows the elapsed time of the test runs.

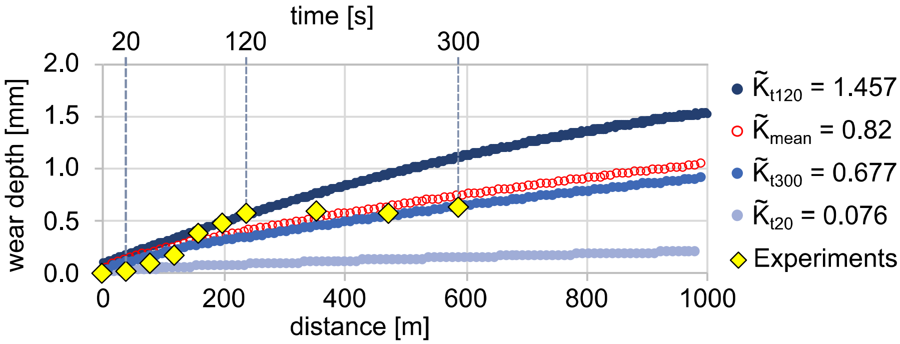

Figure 7: Maximum wear depths resulting from FE analysis using different coefficients $\widetilde{K}$ compared to experimental measurements

As explained in Section 1.3, the coefficients were calculated using experimental results obtained after different test durations, and therefore after different distances travelled. Table 2 lists the numerically determined wear depths for the three coefficients, $\widetilde{K}_{t20}$, $\widetilde{K}_{t120}$, and $\widetilde{K}_{t300}$, for the corresponding distances. In addition, the deviation

$$\delta_{\text{wear}}(s) = \frac{d_{\text{wear\_exp}}(s) - d_{\text{wear\_num}}(s)}{d_{\text{wear\_exp}}(s)} \cdot 100\ \% \tag{7}$$

of the numerically determined wear depth $d_{\text{wear\_num}}$ from the experimentally determined depth $d_{\text{wear\_exp}}$ at the distance s is given. Considering the distances used to determine the coefficients, the numerically and experimentally determined wear depths correspond closely. However, as Figure 7 shows, when other distances are considered, the numerically determined wear depth differs significantly from the experimentally determined wear depth. To quantify this, the value

$$\Delta = \frac{1}{9} \cdot \sum_{s} |\delta_{\text{wear}}(s)| \tag{8}$$

calculates the average of the deviations δ_{wear} for all nine distances tested.

Table 2: Comparison of numerical and experimental wear depths using $\widetilde{K}_{t20}$, $\widetilde{K}_{t120}$, and $\widetilde{K}_{t300}$

wear coefficient	s	Numerical $d_{\text{wear\_num}}(s)$	Experimental $d_{\text{wear\_exp}}(s)$	$\delta_{\text{wear}}(s)$	Δ
$\widetilde{K}_{t20}$	39 m	0.021 mm	0.024 mm	13.79 %	72 %
$\widetilde{K}_{t120}$	236 m	0.558 mm	0.567 mm	1.66 %	53 %
$\widetilde{K}_{t300}$	589 m	0.629 mm	0.627 mm	-0.46 %	38 %

As δ_{wear} in Table 2 shows, the FE model accurately reproduces the wear of the FKM material sample at a given distance based on the measurement data used to calculate the wear coefficient. However, Δ indicates that the numerically determined wear depth still differs from the experimentally determined wear depth when the values before and after the data, which were used to calculate the coefficients, are considered.

The maximum wear depth resulting from the FE analysis using the coefficient $\widetilde{K}_{mean}$ was determined for the same distances and compared with the experimental data, Table 3. Using the wear coefficient $\widetilde{K}_{mean}$ results in significantly greater deviations δ_{wear} between the numerically and experimentally determined wear depths. However, the average deviation Δ of 40 % is significantly smaller than that achieved using the coefficients $\widetilde{K}_{t20}$ and $\widetilde{K}_{t120}$.

While the FE analysis results for the coefficients $\widetilde{K}_{t20}$ and $\widetilde{K}_{t120}$ match the measurements at one point, they differ greatly elsewhere. On average, the FE analysis results for the coefficients $\widetilde{K}_{t300}$ and $\widetilde{K}_{mean}$ are closest to the measurement data.

Table 3: Comparison of numerical and experimental wear depths using $\widetilde{K}_{mean}$

wear coefficient	s	Numerical $d_{\mathrm{wear\_num}}(s)$	Experimental $d_{\mathrm{wear\_exp}}(s)$	$\delta_{\mathrm{wear}}(s)$	Δ
$\widetilde{K}_{mean}$	39 m	0.117 mm	0.024 mm	-385.68 %	40 %
$\widetilde{K}_{mean}$	236 m	0.384 mm	0.567 mm	32.28 %	
$\widetilde{K}_{mean}$	589 m	0.722 mm	0.627 mm	-15.19 %	

To measure the wear depth after the test runs, the material samples were positioned centrally beneath the line laser of the IMA-Sealscanner [6], as the greatest wear occurred in the center of the samples. It should be noted that the wear depths shown in Figure 7 resulting from the FE analysis represent the maximum wear depths from all nodes in the FE model rather than the maximum wear depth at the center of the sample. Figure 8 (left) shows the wear depth across the material sample, as well as a zoomed-in view of the contact area. In Figure 8 (right), the scale has been adjusted to show only the wear depth between 1.125 mm and 1.145 mm. Thus, the greatest wear occurs in the center of the sample. Therefore, the wear depths measured at the center of the samples after the experiments are comparable to the numerically determined maximum wear depths.

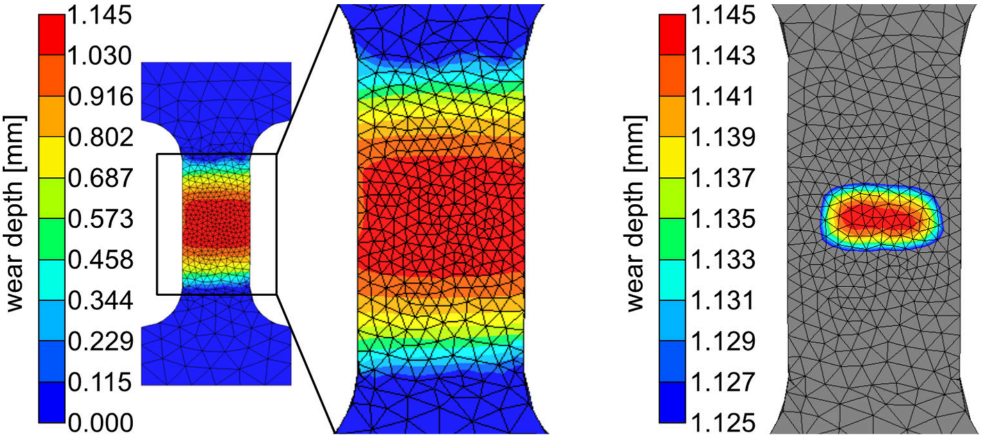

Figure 8: Wear depth in the contact area after 900 m

Figure 9 compares the contact pressure resulting from the FE analysis using the wear coefficient $\tilde{K}_{t300}$ with the contact pressures obtained by measuring the contact area after the experiments. The experimental contact pressures in Figure 9 are the same as those shown in Figure 3. The contact pressures obtained from the experiments correspond very well to the values resulting from the FE analysis.

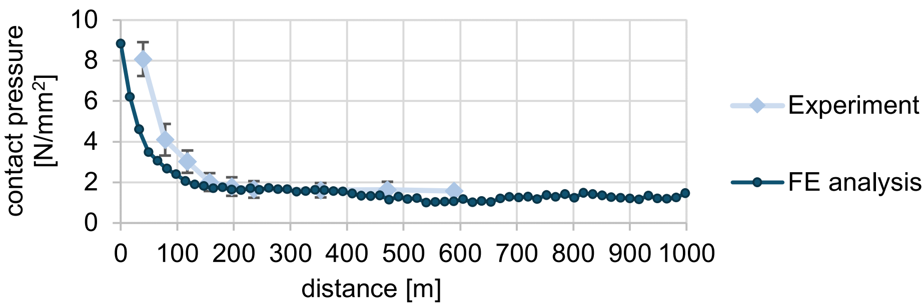

Figure 9: Contact pressure resulting from FE analysis using $\tilde{K}_{t300}$ compared to experiments

2.3 Discussion

Comparing the contact pressure and wear depth obtained from the FE analysis with the experimental results validates the numerical method used to determine wear on the material sample. The results obtained using the wear coefficient $\tilde{K}_{t300}$ agree very well with the experimental data. This enables the wear of the material sample to be determined even over a longer test distance than in the experiments.

The maximum wear depth measured after the experiment was 0.63 mm after 589 m. During longer test runs covering greater distances, the material samples tore, making it impossible to measure the wear depth afterwards. This may have been caused by high temperatures in the contact area. A thermal imaging camera was used to measure temperatures at the contact area from the outside, recording temperatures of up to 125 °C [5]. The FE analysis was able to model wear depths of up to 1.6 mm. However, the FE analysis provides only a simplified representation of real tribological behavior and therefore does not account for all the effects, such as material failure caused by high temperatures. Nevertheless, the FE analysis allows wear to be approximated over a long period of time, even though tests of such duration have not been conducted.

Using the wear coefficient $\widetilde{K}_{t20}$, which was calculated based on 20-second test data, the FE analysis yielded a wear depth of 0.2 mm over a distance of 1,000 meters. Using the wear coefficient $\widetilde{K}_{t120}$, which was calculated based on 120-second test data, the wear depth after 1,000 meters was almost eight times greater, at 1.55 mm. This highlights the importance of high-quality experimental data and the precise determination of the wear coefficient.

To avoid underestimating the wear coefficient due to a smaller wear rate in the beginning or to avoid overestimating the wear coefficient due to the higher wear rate during the running-in phase, the longest test run was assumed to be the most accurate basis for determining the wear coefficient. As expected, the $\widetilde{K}_{t300}$ coefficient, which was determined from data obtained in the longest test run, produced the smallest average deviation between the experimental data and the results obtained from the FE analysis.

In the experimental setup, the contact conditions evolve significantly over time. Initially, there is line contact, which causes high localized contact pressures of approximately 8 N/mm². This rapidly broadens the contact area, reducing normal pressure to approximately 1.6 N/mm². Furthermore, the temperature rises at the beginning of a test run, which alters the elastomer's stiffness and wear resistance. Consequently, the wear coefficient varies over time and the wear determined by the numerical method strongly depends on the duration of the tests used to calculate the wear coefficient. Therefore, while the numerical method can accurately represent the wear at a given point in time, it deviates significantly for shorter or longer sliding distances.

Although advanced wear models incorporate pressure exponents and thermal activation terms, they require a larger number of empirical parameters. To reliably determine these additional coefficients, extensive experimental studies are needed that systematically investigate various influencing factors. The main objective was not to create an increasingly complex wear model, but to develop and verify the numerical method (for example the integration of the subroutine and the remeshing strategy) and to assess the applicability of the standard Archard model based on fast and straightforward experiments using the modified Brugger measuring device.

2.4 Transfer to a sealing ring

The wear coefficients were transferred to a 2D FE model of a rotary shaft seal, in which the mounting of the sealing ring and the rotation of the shaft were modeled. After a sliding distance of 300 km, the numerically determined wear widths at the sealing edge range from 0.35 mm ($\widetilde{K}_{t20}$) over 1.26 mm ($\widetilde{K}_{t300}$) to 1.93 mm ($\widetilde{K}_{t120}$). Figure 10 shows the mounted, worn sealing edges after 300 km for the three wear coefficients. The same remeshing method was used as in the FE model of the measuring device, which resulted in different mesh sizes at the sealing edge.

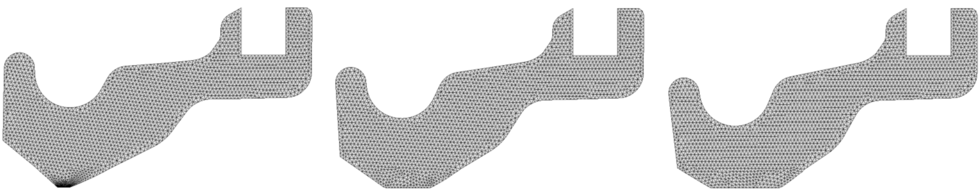

Figure 10: 2D FE analysis: worn sealing ring using $\widetilde{K}_{t20}$ (left), $\widetilde{K}_{t300}$ (middle) and $\widetilde{K}_{t120}$ (right), mounted on the shaft

After mounting the sealing ring onto the shaft, the FE analysis revealed a radial force of 36 N. This was followed by rotation of the shaft over a distance of 300 km, which resulted in radial forces of 35.9 N ($\widetilde{K}_{t20}$), 27.3 N ($\widetilde{K}_{t300}$) and 13.6 N ($\widetilde{K}_{t120}$) after 300 km. Therefore, depending on the duration of the experimental tests used to determine the wear coefficient, the radial force and wear width can vary significantly. This emphasises the importance of accurately determining the wear coefficient. If the wear coefficient is not validated or is determined incorrectly, the numerical method may produce highly inaccurate results.

3 Summary and Conclusion

In this study, a numerical method was developed to predict the wear of material samples and rotary shaft seals using the finite element analysis software Marc/Mentat and a Fortran subroutine. Experimental wear tests were conducted under unlubricated conditions using FKM material samples to determine the material-dependent wear coefficient for a linear wear model. As wear depth does not increase linearly with the distance travelled, multiple wear coefficients were calculated depending on the duration of the respective test runs. To validate these coefficients, an FE model of the test setup was built to reproduce the wear determined experimentally. Finally, the calculated wear coefficients were transferred to a 2D FE model of a rotary shaft seal to determine wear and the resulting radial forces after a long sliding distance.

The results demonstrate that the numerically predicted wear strongly correlates with the experimental data when the appropriate wear coefficient is used. The coefficient determined from the longest test run ($\widetilde{K}_{t300}$) provides the most accurate prediction, as it avoids overestimation of wear due to the initial running-in phase of the material.

This study highlights the critical importance of precisely defining and validating wear coefficients. As demonstrated by the transfer to the actual sealing ring, the use of an unvalidated or incorrectly determined coefficient results in highly inaccurate numerical predictions of wear and, consequently, of radial force. As failure of rotary shaft seals due to wear can result in costly system breakdowns, the numerical method and approach for validating the calculated wear coefficient presented in this study provide a foundation for accurately predicting seal behavior.

The next step is to use the numerical method presented in this paper to determine the wear of rotary shaft seals, and to compare the results with test bench experiments. To this end, the measuring device's shaft was replaced to ensure that its surface specifications matched those of the test bench shafts. The tests to determine the wear coefficient and the experiments with rotary shaft seals on the test bench will both be performed under lubricated conditions.

4 Nomenclature

Variable	***Description***	***Unit***
A_{wear}	wear area	mm^2
d_{wear}	wear height	mm
$d_{\mathrm{wear\_exp}}$	experimentally determined wear depth	mm
$d_{\mathrm{wear\_num}}$	numerically determined wear depth	mm
δ_{wear}	deviation	%
e^*	hypothetical friction energy density	J / m^3
F_{N}	normal force	N
H	material Hardness	N / mm^2
K	wear coefficient Archard model	-
$\widetilde{K}$	wear coefficient	mm^2 / N
k_{b1}	coefficient in Bayer wear model	
k_{b2}, k_{b3}	exponents in Bayer wear model	-
k_{w1}	coefficient in Weber wear model	-
k_{w2}	exponent in Weber wear model	mm^2 / N
p_{N}	normal Pressure	N / mm^2
s	sliding distance	mm
v_{rel}	relative velocity	mm / s
V_{wear}	wear volume	mm^3
W_{fric}	friction work	N m
μ	coefficient of friction	-

5 References

[1] Fleischer, G.: *Energetische Methode der Bestimmung des Verschleißes*, Schmierungstechnik 4, vol. Nr. 9, pp. 269-274, 1973.

[2] Daubner, A.: *Analyse, Modellierung und Simulation von Verschleiß auf mehreren Skalen zur Betriebsdauervorhersage von Wellendichtringen aus PTFE-Compound*, Dissertation, University of Stuttgart, ISBN 978-3-936100-56-3, 2014.

[3] Haiser, H. B.: *PTFE-Compounds im dynamischen Dichtkontakt bei druckbelastbaren Radial-Wellendichtungen*, Dissertation, University of Stuttgart, ISBN 3-921920-97-3, 2001.

[4] Weber, D.: *Numerische Verschleißsimulation auf Basis tribologischer Untersuchungen am Beispiel von PTFE-Manschettendichtungen*, Dissertation, University of Stuttgart, ISBN 978-3-936100-40-2, 2012.

[5] Gerhard, J.; Hörl, L.; Bauer, F.: *Brugger Test Redefined: Accelerated Wear Analysis of Sealing Materials*, 23rd International Sealing Conference 2026, Stuttgart, Germany, https://doi.org/10.61319/1ZV6DE1J, 2026.

[6] University of Stuttgart - Institute of Machine Components: *IMA-TechSheet #102050 V2*, available at https://www.ima.uni-stuttgart.de/dokumente/forschung/dichtungstechnik/einrichtungen/en/102050en.pdf, accessed on April 9, 2026.

6 Authors

University of Stuttgart, Institute of Machine Components (IMA)
Pfaffenwaldring 9, 70569 Stuttgart, Germany:

Jacqueline Gerhard, M. Sc., ORCID 0000-0002-4879-5653,
jacqueline.gerhard@ima.uni-stuttgart.de

Frank Bauer, apl. Prof. Dr.-Ing., ORCID 0000-0001-7799-7628,
frank.bauer@ima.uni-stuttgart.de

https://doi.org/10.61319/IEL91I7J